Delocalization of the Fe 3*d* levels in the quasi-two-dimensional correlated insulator $FePS_3$

Won-Kook Choi, E. Kneedler, and S. D. Kevan*
Physics Department, University of Oregon, Eugene, Oregon 97403
(Received 19 January 1994; revised manuscript received 11 July 1994)

The degree of spatial localization of the Fe 3*d* levels in the quasi-two-dimensional correlated insulator iron phosphorus trisulphide ($FePS_3$) is probed using resonant and angle-resolved photoemission in the range $h\nu = 40 \sim 65$ eV. Our results indicate that the 3*d* levels in this compound are not as localized as assumed by an existing ionic model. Spectra can be adequately fitted using an atomic multiplet theory for the $3d^{n-1}$ final state modified by the presence of an octahedral ligand field. However, a relatively low Racah exchange parameter $B = 0.075$ eV is deduced and is interpreted in terms of greater hybridization with neighboring sulfur atoms than in iron oxides and halides. Resonant photoemission spectra collected near the iron *M* edge yielded excitation spectra composed of three prominent peaks approximately characterized by Fano line shapes. Systematic variation of the Fano asymmetry parameter *q* through the 3*d* multiplet is attributed to differential hybridization of various Fe 3*d* levels with sulfur 3*d* orbitals. Finally, we report angle-resolved photoemission results in the mirror symmetry planes, which indicate that some components of the 3*d* multiplet are substantially delocalized by band formation parallel to the layers. We summarize and discuss these results in terms of the covalency of this material.

I. INTRODUCTION

The discovery of the high-temperature cuprate superconductors has lead to enormous scrutiny of materials that exhibit reduced dimensionality and have electronic structures in which electron correlation plays a significant role.[1,2] $FePS_3$, a prototypical member of the MPX_3 transition-metal phosphorus trichalcogenide series of compounds, bears qualitative similarity to the cuprates in these respects.[3,4] Similar to the cuprates and other systems having correlated electronic structures, an important issue in the MPX_3 compounds concerns the degree of spatial localization of the 3*d* manifold. This in turn is determined by the relative importance of on-site correlation and exchange interactions, crystal-field splittings, and hybridization with neighboring atoms. Such materials are commonly modeled using simple phenomenological parameters—a correlation energy, a crystal-field parameter, and a hopping or charge-transfer integral, for example. These models mask much of the underlying complexity associated with quenching and/or delocalization of atomic multiplets. This paper presents the results of resonant photoemission (RESPES) and angle-resolved photoemission (ARP) studies of $FePS_3$ to probe the degree of localization of the 3*d* levels.

The MPX_3 materials are structurally similar to the MX_2 transition-metal dichalcogenide layered compounds and thus exhibit many quasi-two-dimensional (2D) behaviors.[5] One third of the MX_2 metal atoms are replaced in the MPX_3 compounds by phosphorous dimers. Each trilayer is composed of a covalently bonded hexagonal network of $(P_2X_6)^{4-}$ ions intersecting a honeycomb of formally divalent M^{2+} ions. The transition-metal atoms are coordinated to six chalcogen atoms in distorted octahedral symmetry. Unlike the MX_2 compounds where the one-electron approximation provides a reasonable zero-order description of electronic properties, the 3*d* transition-metal analogs of the MPX_3 series are correlated antiferromagnetic insulators in their ground states.

An ionic model for the electronic structure of the MPX_3 compounds has been developed, largely through the work of Khumalo and Hughes,[6] and Piacentini *et al.*,[7,8] in which the 3*d* manifold remains localized and noninteracting. The dominant splittings of the 3*d* manifold involve the crystal field and multiplets formed by electron correlation. A simplified energy level diagram for $FePS_3$ is shown in the left part of Fig. 1. The atomic 3*d* level [panel (c)] is split by a global exchange energy *U* [panel (b)] and then the t_{2g} and e_g levels are further split by a crystal-field $10Dq$ estimated to be ~ 10 eV [panel (a)].[9,10] The trigonal distortion to D_{3d} symmetry further splits the t_{2g} levels into a_{1g} and e_g sets separated by 0.23 eV (not shown in Fig. 1).[10] Local moments on each metal center are weakly ferromagnetically or antiferromagnetically coupled to neighboring sites, leading in all known cases to antiferromagnetic ground states with Néel temperatures of 100–300 K.[11] This model, which successfully explained optical and soft x-ray absorption results,[6–8,12,13] is consistent with the observed nearly integral magnetic moments on the transition-metal centers in the paramagnetic region,[11,14,15] and has provided useful insight into understanding the systematic variation in the ability of these compounds to intercalate alkali-metal atoms.[14] Lattice-dynamics calculations also suggest the importance of metal-P_2X_6 interactions.[16]

The ionic model is not adequate to explain other spectroscopic results, particularly the degree of mixing between transition metal 3*d* and anion ligand states and the structure of the lower conduction band of $FePS_3$ observed in inverse photoemission results.[17] Also, the 3*d* bandwidths of MX_2 compounds are typically 0.5–1.0 eV, and this should not be dramatically smaller in the MPX_3 compounds. Extended Hückel molecular-orbital calculations[18,19] indicate significant mixing between M 3*d* and S

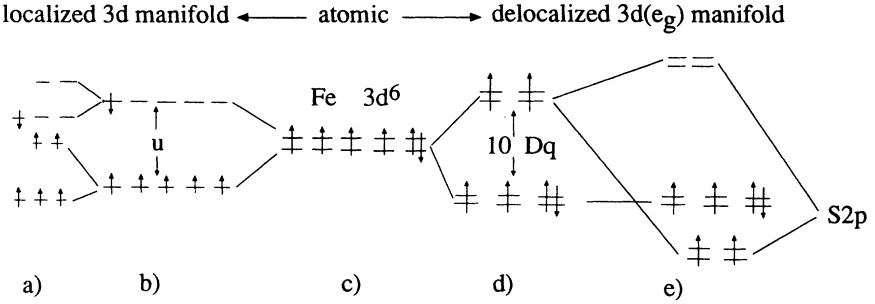

FIG. 1. Schematic representation of two simple models for the electronic structure of $FePS_3$. Panel (c) represents the unsplit $3d^6$ level. Moving left from this panel emphasizes electron exchange and correlation. Panels (b) and (a) add an on-site correlation energy U and the crystal-field interaction $10Dq$, respectively. Hybridization is emphasized and correlation is neglected in the panels to the right of panel (c). The crystal field first splits the $3d$ manifold in panel (d), and strong e_g-S $3p$ hybridization further splits the e_g levels into bonding and antibonding sets in panel (e).

$3p$ states. This mixing occurs preferentially with e_g levels since these are directed toward the octahedrally coordinated sulfur ligands. The dominant splitting in these calculations is thus associated with formation of bonding and antibonding Fe $3d$ (e_g)–S $3p$ levels, as shown in panels (d) and (e) in Fig. 1, and electron correlation interactions are largely ignored.

It is likely that the true situation lies intermediate between these two models and that correlation, crystal field, and hybridization are all important. In principle, *ab initio* self-consistent band calculations can help clarify the situation. These order the $3d$ levels as in panel (a) of Fig. 1 with some additional width due to band formation, in qualitative support of an intermediate model.[20,21] In the calculations, preferential hybridization of the sulfur orbitals with the e_g relative to the t_{2g} levels is not readily apparent, since the ordering of the t_{2g} and e_g spin-down levels is not reversed due to formation of a strong Fe $3d$ (e_g)-S $3p$ bonding level. These calculations were based upon the local-density approximation, and the application of this technique to such highly correlated systems is not without problems. For example, the calculated ground state of $FePS_3$ is metallic, in gross contradiction of experiment where a correlation gap of ~ 1.5 eV is observed.[9,22,23]

The most direct probes of electronic structure, photoemission, and inverse photoemission have been usefully applied to try to elucidate the compounds' electronic structures.[9,12,24] Presence of a highly localized $3d$ shell normally will lead to RESPES at photon energies just above the threshold for $2p$ or $3p$ core excitation. This motivated one previous RESPES study and, indeed, some features were observed to resonate in intensity and were assigned to $3d$ levels and satellites.[24] While these results certainly imply some localized character, the delicate interplay between localized and delocalized effects were not seriously examined. To date, no ARP measurement of any MPX_3 compound has been reported. The primary purpose of the present experiment was to undertake RESPES and ARP measurement of $FePS_3$ to examine this interplay in detail.

In the following sections, we report the photoemission spectra for $FePS_3$ and determine the most appropriate model for this compound's electronic structure. We start by relating our observed spectral features to the various iron-, sulfur-, and phosphorous-derived levels. The iron-derived features in the spectra are then modeled in terms of the $3d^{n-1}$ final-state ionization potentials and the Racah B and C parameters using the Tanabe-Sugano diagram.[25] We find that the spectra can be adequately fitted within this localized model, but that the Racah parameters are substantially smaller than for other more ionic iron compounds. This is consistent with a greater degree of hybridization in $FePS_3$. Excitation spectra corresponding to the Fe $3d$ states, the satellites, and the sulfur $3p$ states are then presented and are decomposed into Fano resonance lines. Systematic variation of the Fano asymmetry parameter q indicates differential Fe $3d$–S $3p$ hybridization. We discuss the relationship between our excitation spectra and recent inverse photoemission (IP) spectra[17] as well as $M_{2,3}$ absorption-edge spectra[13] to clarify the position of the empty $3d$-derived valence states. Finally, we report the quasi-2D electronic structure of $FePS_3$ determined using ARP along the symmetry lines of the $FePS_3$ Brillouin zone at various photon energies to provide further information about the localization of the $3d$ levels. These results also are interpreted in terms of significant delocalization of part of the $3d$ multiplet. We conclude with a discussion of the covalency of $FePS_3$ and suggest useful ways to think about its electronic structure. Throughout this analysis, we compare the valence electronic structure and the covalency of $FePS_3$ to those of other ionic iron compounds to determine the relative extent of localization of the iron levels.

II. EXPERIMENTAL PROCEDURES

The $FePS_3$ crystals were grown using the chemical vapor transport method[26] and were lustrous black, opaque plates of hexagonal shape. The samples were very flexible and much care was taken to avoid deformation upon mounting. A clean surface of $FePS_3$ was attained by cleaving *in situ*. In order to establish electrical contact, high purity silver paint (SPI Co.) was daubed between the crystal and sample holder. After curing at 150–180 °C for 30 min, electrical contact was examined and the edges of the crystal were trimmed so that the samples had an

approximately circular shape with a diameter of about 5 mm. The edge of the crystal was prone to bend after cleaving so that photoelectrons were hindered from exiting the surface uniformly. A small percentage of the cleaves provided enough flat space ($\sim 1 \times 2$ mm^2) with adequate electrical contact that photoemission experiments could be accomplished. After cleaving, the cleanliness and azimuthal orientation of the crystal were identified using Auger electron spectroscopy and low-energy electron diffraction, respectively. The surfaces remained clean and ordered for several days in our vacuum system. In order to locate the position of the Fermi level and to investigate the reaction of the Fe $3d$ state with the adsorption of alkalis, potassium was dosed using a getter evaporation source (SAES, Inc.). It was dosed at room temperature and at a pressure of $5.5 \sim 6.5 \times 10^{-10}$ torr. The high angular and energy resolution ARP experimental system has been described in detail previously.[27,28] Experiments were accomplished at the National Synchrotron Light Source at Brookhaven National Laboratory, using 6-m toroidal grating monochromator. The total energy and angular resolutions used here were typically less than 150 meV and 1°, respectively, at full width at half maximum.

III. RESULTS AND DISCUSSION

Figure 2 provides normal emission energy distribution curves (EDC's) of $FePS_3$ collected at a variety of photon energies near the $3p$ threshold. The intensities of all EDC's are normalized to the photon current. That little dispersion is observed in these features as a function of photon energy reflects the 2D character of these materials. The high-energy onset of the spectra [i.e., the valence-band maximum (VBM)], was located at a binding energy (BE) of ~ 1.5 eV relative to E_F. As is normally done in photoemission studies of traditional semiconductors, we measure the binding energies of various spectral features relative to the VBM.

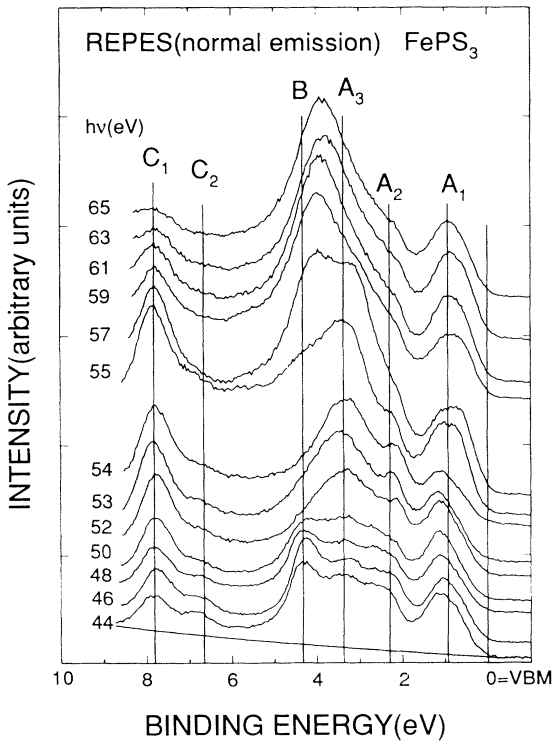

FIG. 2. Normal emission energy distribution curves of the valence bands of $FePS_3$ at several photon energies $h\nu$ in the vicinity of the Fe $3p$ threshold energy. The different vertical lines correspond to the assignments after Ref. 24. Features $D-G$ are discussed in more detail in Ref. 24.

A. Photoemission peak assignments

Our spectra are largely consistent with Piacentini's results,[24] albeit with slightly better definition of some features. Some small differences may be attributed to the different angular acceptance of their energy analyzer. Piacentini *et al.*, assigned most features observed in the valence band by comparison to a calculated densities of states, and we adopt their assignments and lettering. The peaks A_1, A_2, and A_3 are similar to features on ionic iron oxides and chlorides[29,30] and are taken to be primarily derived from the final-state multiplet splitting of the Fe $3d$ states. Peaks B, C_1, and C_2 are located where the sulfur and phosphorous $3p$ bonding manifolds are expected. However, the large intensity variation of the peak C_1 is more characteristic of an Fe $3d$-related feature. The ratio of the calculated atomic subshell photoionization cross sections is small ($\sigma_{3p}/\sigma_{3d}) = 0.07 \sim 0.1$) in the range of $40 \sim 60$ eV,[31] so that the contribution of $3d$ electrons should dominate the EDC's. Piacentini *et al.* concluded that peak C_1 is a satellite of the main lines.[24] We caution, however, that the significant energy dispersion of this feature reported in Sec. III C is contrary to this conclusion. Other sulfur and phosphorous levels are observed (but not shown) at higher binding energy, in accord with Piacentini's results.[24]

The P $3p_z$ level primarily responsible for the covalent bonding of P_2 dimer is not easily associated with features in any of our spectra. This level, which must play a crucial role in determining the structural stability of these phases, was suggested to lie at the top of the valence band in the ionic model.[8] In calculations,[21] however, the crystal-orbital overlap population curve for $P-P$ shows that one peak among three $P-P$ bonding levels is located in the region containing strong metal t_{2g} orbitals. In either case, emission from this feature would probably be masked by the more intense and overlapping Fe $3d$ features.

1. Fe 3d main lines and satellites

Distinct changes in the shape of the EDC's in Fig. 2 occur near the Fe $3p$ threshold at $h\nu = 55$ eV. These arise from the resonance between the $3p$ inner shell excitation and the valence $3d$- and $4s$-shell excitations. Peaks A_3 and C_1 resonate in intensity most prominently relative to other peaks in the EDC's. The behavior of such features can be analyzed to provide additional information about the material's electronic structure, as discussed in Sec. III B.

As discussed above, the peak C_1 lies well below the VBM and is probably not associated with direct emission from a predominantly Fe 3*d* level since this would require a 3*d* bandwidth in excess of 10 eV. The 3*d*-related character in C_1 must arise from another cause, i.e., multielectron shake up. Similar satellites were observed in x-ray photoemission spectroscopy (XPS) studies of the Ni 2*p* level in $NiPS_3$ located 5 and 10 eV below the main line.[7,32] The Fe 2*p* XPS spectrum of $FePS_3$ exhibits a broad and strong satellite at each spin-orbit component and the two main lines themselves appear quite asymmetric and broad.[7]

These kinds of satellites can be ascribed to either a multielectron excitation (shake up) process[33] or anion ligand-to-metal monopole charge-transfer transitions.[34,35] In the former process, the satellites are caused by simultaneous excitation of a second 3*d* electron to unoccupied 4*s*, 4*p*, or 3*d* levels upon photoemission. Charge-transfer transitions are often invoked to explain the observed satellites of the less ionic transition-metal oxides like NiO and CoO. Given the close proximity of the chalcogen levels and the low ionicity of the MPX_3 phases relative to, e.g., oxides and halides, we believe that this satellite is probably of the charge-transfer variety.

2. *Multiplet splittings in the Fe 3d manifold*

The qualitative analysis in the previous section begged the issue of the precise relationship between the spectral features in Fig. 2 and final state Fe 3*d* multiplet splittings. We now attempt to apply a relatively straightforward model to our spectra with the goal of achieving this relationship.[36,37] The model treats the iron centers to be isolated, yet subject to an octahedral crystal field characterized by the parameter $10Dq$. We neglect the splitting of the t_{2g} manifold due to the small trigonal distortion, and the multiplet splittings of the e_g and t_{2g} manifolds are evaluated for the final state (i.e., Fe^{3+}) in terms of the Racah *B* and *C* Coulomb and exchange parameters.

The direct photoionization of a 3*d* electron leaves an Fe^{3+} ion with a sextet ground state ${}^6S({}^6A_{1g})$ and three lowest quartet excited states, ${}^4G$, ${}^4D$, ${}^4P$.[38] In an octahedral field, the ${}^4G$ state of the free ion splits into two threefold-degenerate states ${}^4T_{1g}(t_{2g}^4e_g^1)$ and ${}^4T_{2g}(t_{2g}^4e_g^1)$, a doubly degenerate state ${}^4E_g(t_{2g}^3e_g^2)$, and a nondegenerate state ${}^4A_{1g}(t_{2g}^3e_g^2)$. The ${}^4D$ state of the free ion splits into a doubly degenerate state ${}^4E_g(t_{2g}^3e_g^2)$ and a triply degenerate state ${}^4T_{2g}(t_{2g}^3e_g^2)$, while the ${}^4P$ state of ion will be left triply degenerate, ${}^4T_{1g}(t_{2g}^3e_g^2)$. The photoemission selection rules allow final states to have the above symmetries in the $3d^5$ high-spin configuration, and these states lie within the expected energy window of our experiment.[38] In the absence of any trigonal distortion, the levels ${}^4A_{1g}$ and ${}^4E_g$ are exactly degenerate. Although this degeneracy will be lifted by the trigonal distortion in $FePS_3$, the magnitude of the splitting of 60 meV (Ref. 39) is so small that the separation was neglected. In addition, the ${}^4E_g(t_{2g}^3e_g^2)$ multiplet of ${}^4D$ free-ion state was excluded from the final states since it is forbidden by the exclusion principle, at least for an octahedral crystal field.

In treating the data, smooth backgrounds were first subtracted from the raw EDC's. Thereafter the spectral feature *B* was removed from the curves by subtraction of a simple Lorentzian line. In this way, multiplets derived from iron 3*d* states and *p*-band structure (dotted lines in the top panel of Fig. 3) were approximately separated and could be modeled without consideration of atomic subshell cross-section variation. The decomposed multiplet structures extend 5~6 eV below the VBM, comparing well with a width of 5~7 eV ultraviolet photoemission spectroscopy studies of similar iron compounds.[29,30,40] Multiplet curves were considered to be composed of purely 3*d* final states and were fitted using the Tanabe-Sugano diagram.[25] The well-resolved peak around 1-eV BE spectra can be interpreted to be mainly the ${}^6A_{1g}$ ground state. The integrated intensity of this peak relative to that of the rest of the final states, i.e., sextet to quartet states, is 1:3.78, comparing well to the statistical ratio of 1:4.

The spectrum was fitted as Racah parameters and crystal-field parameter ($10Dq$, *B*, $\gamma = C/B$) were varied. The widths of all spectral features were fixed to the same value, and this value was also optimized in the fit. The relative intensities of the multiplets were fixed at statistical values. The resulting best fit of the spectrum at $h\nu = 40$ eV is shown in the bottom panel of Fig. 3. The

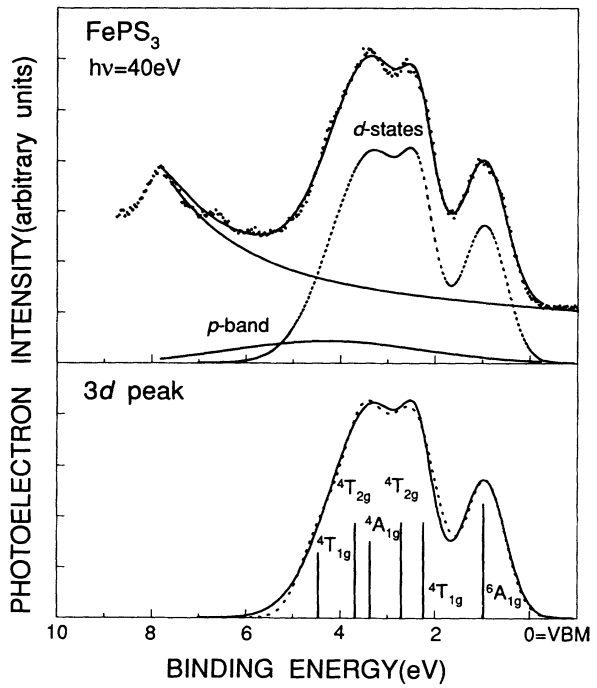

FIG. 3. Energy distribution curve of $FePS_3$ at $h\nu = 40$ eV. Upper panel: The two dotted lines correspond to the contribution of Fe 3*d* states and sulfur 3*p* band, while the dash-dotted line is an approximate background. The solid curve is the best fit to the spectrum. Bottom panel: Best fit to the Fe 3*d* multiplet using the model described in the text. The vertical lines show the calculated $3d^{n-1}$ final-state ionization potentials and intensities for a crystal-field splitting $10Dq = 1.4$ eV, Racah parameters $B = 605$ cm^{-1}, and $C = 2662$ cm^{-1}. Best fit is for a linewidth of 0.98 eV for each multiplet.

derived parameters, $B=605$ cm^{-1} (0.075 eV), $\gamma=4.4$, and $10Dq=1.4$ eV, are all quite reasonable as compared to previous results on related systems. These parameters lead to the following set of final-state ionization potentials (energies in eV with respect to $^6A_{1g}$ level): $^6A_{1g}[\equiv 0$ eV], $^4T_{1g}[1.27]$, $^4T_{2g}[1.74]$, $^4A_{1g}[2.4]$, $^4E_g[2.4]$, $^4T_{2g}[2.72]$, and $^4T_{1g}[3.49]$. A linewidth of 0.98 eV for all multiplets gives the best fit to the spectrum.

Given that this is a simplistic model and also that there are obvious limitations with our treatment of the data (e.g., the background subtraction and removal of the spectral feature B), one should not place too much emphasis on the quantitative results given above. It is interesting, however, to compare the derived value of the Racah parameter B with that of other formally divalent iron oxide and halide compounds and the Fe^{3+} free-ion value. These are given in Table I. The value of the B parameter in $FePS_3$ is 60% of Fe^{3+} free-ion value and is systematically smaller than that of other ionic iron compounds. A parameter β is often defined as the ratio of B in a compound to B_0 in the free ion.[41] The β values, also given in Table I, decrease in magnitude successively. These observations suggest that a larger S $3p$–Fe $3d$ hybridization exists in $FePS_3$, since this would delocalize the $3d$ electrons and thereby reduce the associated Coulomb and exchange integrals. We thus conclude that the $3d$ orbitals in $FePS_3$ are less localized than these other formally Fe^{2+} compounds.

B. Excitation spectra

Figure 4(b) presents excitation spectra, defined as the excitation-energy dependence of the photoemission intensity, for various structures in the EDC's in Fig. 2. The partial-yield spectrum, which represents the optical-absorption spectrum, is shown for comparison in Fig. 4(a).[24] The intensities in the spectra shown in Fig. 4(b) are obtained as the heights of each structure in the raw EDC's after subtracting smooth backgrounds represented by dotted line shown in Fig. 2. Undoubtedly, some errors arise from overlap of adjacent structures and uncertainty in the background subtraction. This is particularly true for features A_3 and B. However, a careful decomposition of the overlapping band using a nonlinear fit to the EDC's could not be achieved without comparable uncertainty.

The five excitation spectra in Fig. 4(b) exhibit distinct similarities to the yield spectrum in Fig. 4(a) and also to recent IP spectra.[17] A subset of three prominent peaks (γ,δ,η) above and two minor peaks (α,β) below $h\nu=54$ eV is observed in each spectrum. Here we focus on the prominent peaks since these provide the most useful information and are the best-characterized in our spectra. Some of the excitation spectra do not exhibit all five peaks, and in some instances (e.g., the γ and δ peaks for curve A_1) the spectra show one broad peak ($\gamma\delta$) instead of two. IP spectra of $FePS_3$, which probe the unoccupied valence bands, exhibited two peaks, which were assigned to $3d$ states.[17] One was close to E_F and was assumed to have t_{2g} orbital symmetry and the other was about 2 eV higher and was assumed to have mixed e_g and S $3p$ character. These two peaks should correspond to the γ and δ in our excitation spectra, and the separation of 2 eV in energy agrees very well with our results. The relationship of the third feature above threshold (η) to the inverse photoemission spectrum is not apparent. Given the analysis in the previous section, these features ought to be interpreted in terms of the multiplet structures for the $d^{n+1}=d^7$ system since an electron has been added to the valence band. We have not attempted to undertake this analysis.

The resonance in the intensity of the satellite structure

TABLE I. The Racah parameters B and C, their ratio γ, and the ratio of the Racah B parameter to the free-ion value (β) for the octahedrally coordinated Fe^{3+} ion in different compounds.

Fe^{3+} in:	B (cm^{-1})	C (cm^{-1})	γ	β	Ref.
Free ion	1015	4800	4.73	1.0	38
Fe_xO	913	4320	4.73	0.9	49
	800	3737	4.67	0.78	40
	629	2805	4.46	0.62	29
$FeCl_2$	661	2962	4.48	0.65	30
$FePS_3$	605	2662	4.4	0.6	present work

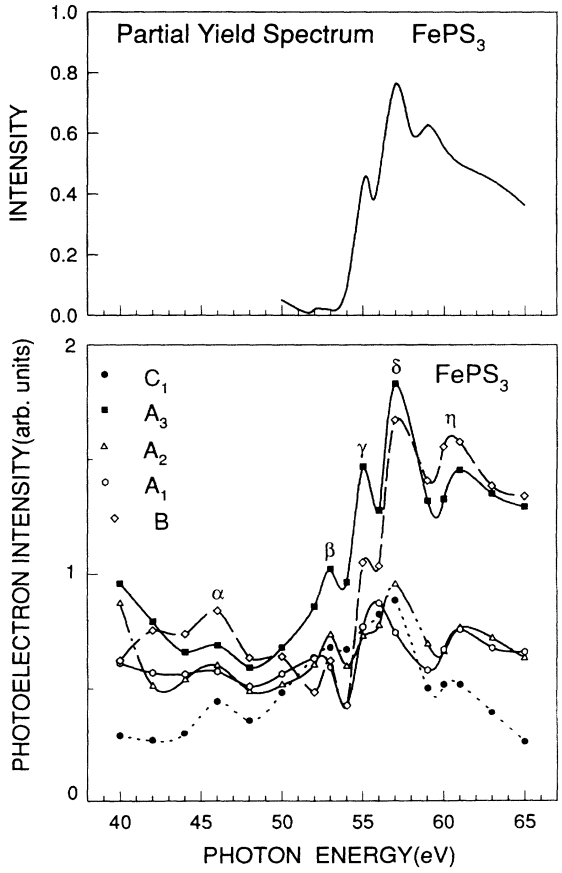

FIG. 4. Bottom panel: Excitation spectra for the main structures in the energy distribution curves of $FePS_3$ in Figs. 1 and 2. Notation is the same as in Fig. 2. For comparison we show the Fe $3p$ partial yield spectrum of $FePS_3$ from Ref. 24 in the upper panel.

C_1 in Fig. 2 is closely related to a Koster-Kronig or super-Koster-Kronig Auger transition following dipole excitation of a $3p$ core electron: $3p^6 3d^N \underline{nl} \rightarrow 3p^5 3d^N nl \rightarrow 3p^6 3d^{N-1} nl + \in$.[42] This autoionization process interferes with the direct double excitation photoemission process ($3p^6 3d^N \underline{nl} \rightarrow 3p^6 3d^{N-1} nl + \in$) and hence the satellite peak is enhanced through a Fano-like process. The structures seen in the excitation spectra discussed later show asymmetric line shapes and are explained by the Fano line shape induced by this interference effect. We also note that an $M_{2,3}$ VV Auger peak having the same final state as the super-Koster-Kronig transition could not be detected in the valence band near or above the resonant photon energy. This result contradicts the mode by Dietz *et al.*[43] for elemental transition metals that the resonance of the satellite is generally enhanced due to the overlap with the Auger emission. It does, however, coincide with the fact that $M_{2,3}$ VV Auger emission is absent in most insulating transition-metal compounds.[44]

In order to model these excitation spectra from first principles, we would need to calculate the line-shape function and the ratio of transition moments of a $3p$ electron to e_g versus t_{2g} orbitals. The difficulty of this approach leads us to analyze the excitation spectra in Fig. 4(b) in terms of phenomenological Fano interactions. According to Davis and Feldkamp,[42] the excitation spectra can be expressed as

$$N(\varepsilon) = A(\varepsilon) + \sum_j K_j f_j(\varepsilon) \ . \tag{1}$$

Here, ε represents the normalized excitation energy and $A(\varepsilon)$ is a smoothly varying background. The second term is the resonant part where K_j is the amplitude and $f_j(\varepsilon)$ is the line shape of resonance line. The analytical form of function $f_j(\varepsilon)$ cannot be easily determined, but the physical origin of some structures observed in x-ray absorption[45] and excitation spectra[46] for the transition-metal compounds have been related to Fano interaction phenomena. The Fano-type interaction produces a spectral line with its typical resonance and antiresonance features for energies above and below the resonance, and is expressed by the following functional form:

$$f_j(\varepsilon) = \frac{(\varepsilon + q_j)^2}{(\varepsilon^2 + 1)^2} \ , \tag{2}$$

where

$$\varepsilon = (h\nu - h\nu_j)/\Gamma_j \ . \tag{3}$$

In these formulas, $h\nu_j$ is the resonance energy for transition j, Γ_j is the spectral half-width of the autoionized state, and q_j is the asymmetry parameter, respectively. We have fitted our excitation spectra to Eq. (1). We assume the background is constant and a constant q value is used for each spectral feature. Features in each excitation spectrum are extracted and labeled by different $h\nu_j$ and Γ_j. The result of this fitting procedure for the case of A_3 is shown in Fig. 5.

The Fano line parameters for the prominent excitations and the main spectral features are tabulated in Table II. While the resonant energies of the peaks γ and δ are fairly consistent, there is measurable discrepancy for η. This difference may be due to ambiguities in the background subtraction as well as to errors caused by not using the integrated intensities for each peak. The most relevant comparison is among the q parameters for the nearly pure and well-resolved Fe $3d$ feature A_1, the over-

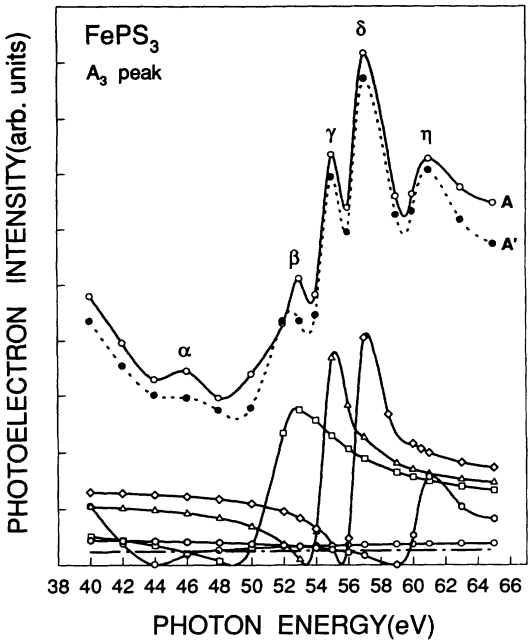

FIG. 5. Decomposition of the A_3 excitation spectrum of $FePS_3$ near the Fe $3p$ threshold. Curve A is the excitation spectrum as measured. The solid curves at the bottom represent the Fano line shapes and a small background, as discussed in the text. Curve A is the sum of these curves and indicates the quality of the fit to the spectrum.

TABLE II. Parameters representing the Fano line shapes obtained by fitting the excitation spectra in Fig. 4. Capital letters correspond to a subset of the peaks in Fig. 2, while Greek letters indicate the prominent peaks in each excitation spectrum.

		$FePS_3$			
		q	Γ	$h\nu_i$	R
A_1	$\gamma\delta$	1.01	1.13	54.88	2.02
	η		1.06	59.95	2.02
A_2	γ	1.33	0.34	54.45	1.12
	δ		0.86	56.20	1.52
	η		0.60	60.89	1.39
A_3	β	1.44	2.08	51.56	2.40
	γ		0.76	54.48	2.54
	δ		0.66	56.54	2.57
	η		0.95	60.34	2.05
B	β	1.46	0.94	52.59	2.87
	γ		0.39	54.71	2.98
	δ		1.00	56.42	3.00
	η		1.71	59.73	2.80
C_i	δ	2.80	1.32	56.33	4.75
	η		0.47	60.33	3.77

lapping Fe $3d$, S $3p$ features (A_3+B), and the satellite C_1. Table II indicates that the q value is larger for the last of these and smallest for the first. This observation can be reasoned qualitatively by the involving hybridization effects. In fact, Kakizaki *et al.*,[46] applied this interpretation to transition-metal chlorides such as $FeCl_2$, $NiCl_2$, and $MnCl_2$. In Eq. (2), the q parameter is given, in the absence of hybridization, as

$$q=\frac{\langle 3p|r|3d\rangle}{\pi V_E\langle \varepsilon l|r|3d\rangle}\ , \tag{4}$$

where $|\varepsilon l\rangle$ is the basis function of the unbound electron, r indicates dipole matrix element, and V_E is the Auger matrix element for autoionization process. Imagine that one sharp state in the multiplet is composed of the hybridization of one Fe $3d$ state and one S $3p$. Then[46]

$$\Psi\approx\frac{1}{(a^2+b^2)}(a|d\rangle+b|L\rangle)\ , \tag{5}$$

where $|d\rangle$ is one of Fe $3d$ orbitals (e_g,t_{2g}) and $|L\rangle$ is a sulfur S $3p$ ligand orbital combination. If this wavefunction form in Eq. (5) is inserted in Eq. (4), the resulting q value is approximately

$$q'=q(1+\gamma)\ , \tag{6}$$

where the covalency parameter γ is defined as $\gamma=b^2/a^2$ and is related to the magnitude of hybridization, but does not represent exactly the degree of covalency. Equation (6) predicts that the q' value should become larger as hybridization increases. The greater q value for the satellite structure than for those derived for Fe $3d$ levels can be also attributed to an increase in the covalency parameter by the inner-core-hole-induced covalency, as discussed previously.[47]

Once again this is a simplistic model and there are obvious limitations with our treatment of the data. Any quantitative conclusions should be viewed with some suspicion. Nonetheless, we find additional qualitative evidence for Fe $3d$–S $3p$ hybridization, that is, the $3d$ orbitals are not so localized as implied by the ionic model. More importantly, this hybridization appears to be different for the different $3d$-related features. We will return to these issues after presenting and discussing ARP results for this compound.

C. ARP studies

The most direct probe of spatial delocalization of the Fe $3d$ orbitals in $FePS_3$ is to search for energy dispersion associated with band formation. For this reason we have measured ARP spectra, a sampling of which is shown in Figs. 6(a) and 6(b). $FePS_3$ adopts a monoclinic crystal structure, but the structure of each layer is hexagonal, with two metal atoms per unit cell in a honeycomb lattice. The spectra in Fig. 6 were collected at momenta along the symmetry lines of this hexagonal unit cell, as shown in the inset in Fig. 6(a). The dimensions of this 2D Brillouin zone (BZ) are 0.703 and 0.608 $Å^{-1}$ along ΓA and ΓY, respectively. The vertical curves through the spectra indicate the dispersion of the primary spectral features A_1, A_2, A_3, B, and C_1. A summary of the derived dispersion relations is given in Fig. 7.

The Fe $3d$ features exhibit different dispersive behaviors. The highest lying feature A_1 is clearly visible in all spectra and exhibits small dispersion (<0.2 eV) throughout the BZ. Feature A_2 also shows little measurable dispersion, although it can be clearly observed only over a narrow range of momenta near the center of the BZ. The primary reason for this is that the more intense feature A_3 exhibits pronounced upward dispersion by nearly 1 eV away from normal emission in both azimuthal directions. The feature labeled C_1 also disperses upward in energy away from zone center and appears to track the energy of feature A_3. That is, there is a roughly constant energy difference of 4.6 ± 0.2 eV between these two features in all spectra. The observed dispersion of feature C_1 contradicts its assignment as a satellite in Sec. III A. The simultaneous observation of a resonance, which implies main-line bandlike character, is an enigma

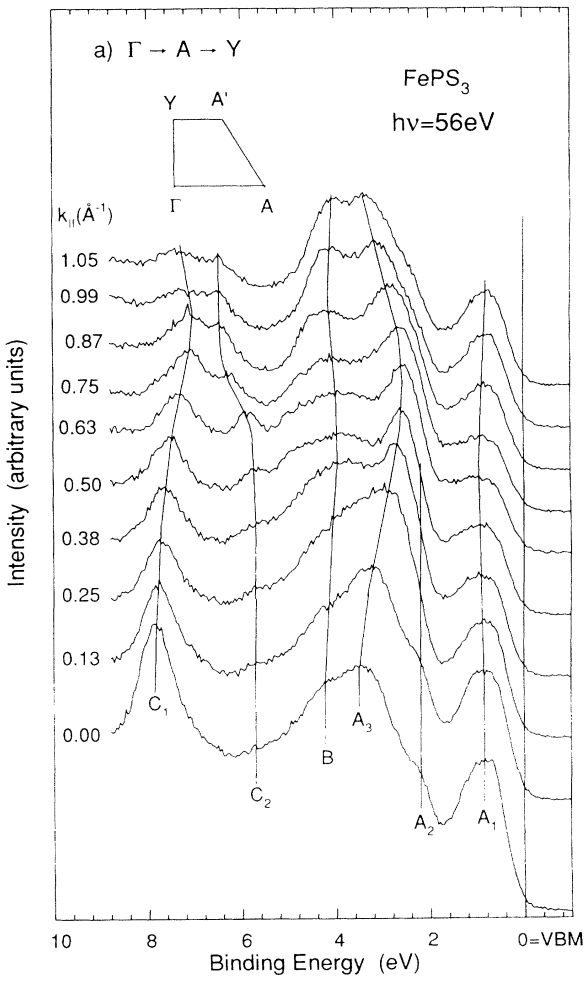

FIG. 6. ARP spectra of $FePS_3$ collected at $h\nu=56$ eV at emission angles in the (a) Γ-A-Y and (b) Γ-Y-Γ directions of the quasihexagonal Brillouin zone. This zone is shown schematically in the inset in panel (a). The wave vectors given are for electrons emitted near the VBM. The vertical lines are included to indicate the dispersion of the primary spectral features.

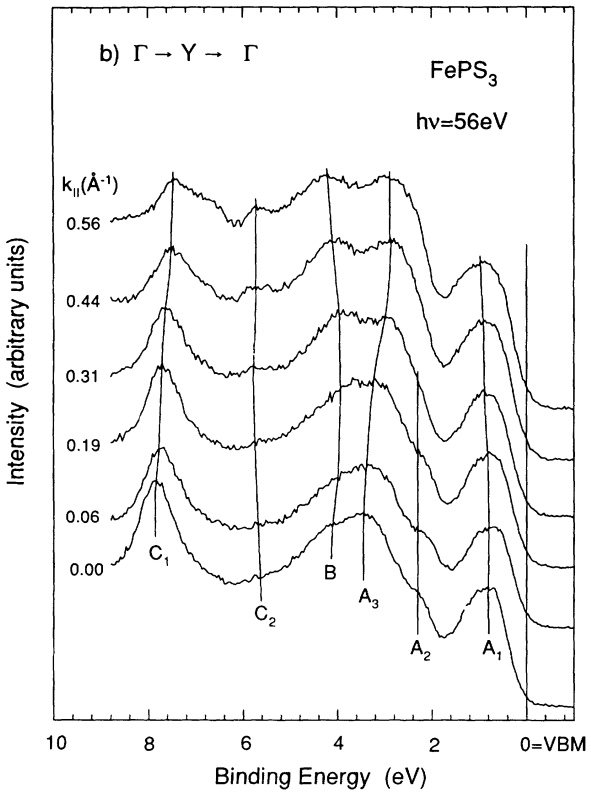

FIG. 6. (*Continued*).

that emphasizes the subtle interplay between localized and delocalized phenomena in this compound. A possible explanation is that feature C_1 is actually composed of two features, one of a nondispersive satellite and the other dispersive phosphorous-sulfur band. However, the satellite intensity should be independent of momentum and one should then presumably see a doubled feature at momenta near the zone boundary. Instead, one sees a single feature with a slowly declining intensity away from zone center.

We make one further observation about feature A_1. In several spectra this feature appears asymmetric. This results from the overlap of more than one peak, as indicated in Fig. 8. This shows a high-resolution spectrum collected at normal emission at $h\nu=56$ eV where the asymmetry is most pronounced and two peaks are clearly resolved. There are several possible explanations for this doubling. From the perspective of atomic multiplet theory, it could result from splitting of the ${}^6A_{1g}$ multiplet by the deviation from octahedral to trigonal symmetry. The observed magnitude of the splitting (0.2 eV) is in good accord with optical measurements.[10] An alternative explanation is based upon the fact that there are two iron atoms per geometric unit cell and more than two for the magnetic unit cell. In terms of hybridization and band formation, one thus naturally expects splitting of the iron-derived bands into bonding and antibonding combinations. Finally, in the phenomenological theories discussed in the Introduction and further in Sec. IV, the splitting could be attributed to a separate 3*d* component produced by crystal-field and exchange splittings. Unfortunately, the splitting was most apparent over a narrow range of momenta and a systematic study was not possible.

IV. DELOCALIZATION OF THE 3d ORBITALS IN $FePS_3$

A. Initial and final states

The discussion in Secs. III A and III B implies some level of applicability of a localized model for the Fe 3*d*

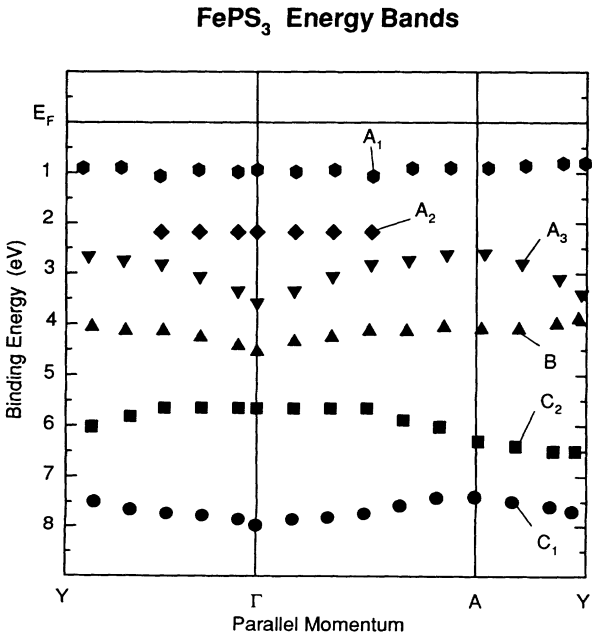

FIG. 7. Summary of the dispersion relations for the primary spectral features in Fig. 6. Bands are labeled as in Fig. 2.

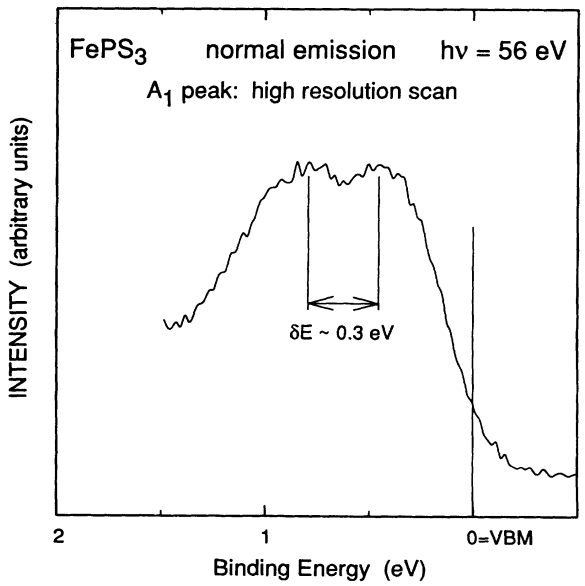

FIG. 8. High-resolution spectrum of the Fe 3*d*-derived feature A_1 near the VBM collected at normal emission and a photon energy of 56 eV. Note the presence of two well-resolved peaks in this feature.

levels in $FePS_3$ since the spectra are adequately reproduced using atomic multiplet theory and the observation of RESPES is closely related to atomic autoionization. Thus it is tempting to relate the three predominantly Fe $3d$ spectral features A_1, A_2, and A_3 to the three lowest levels on the left part of Fig. 1, that is, to $t_{2g}(\downarrow)$, $e_g(\uparrow)$, and $t_{2g}(\uparrow)$, respectively. In the ground state, which is calculated from first principles, associations like this may have some validity. However, the discussion of Sec. III A 2 indicates that this is not really a valid assignment of the photoemission spectra. The spectral features should be considered to arise from the final state $3d^{n-1}$ multiplets, as shown in Fig. 3. In the presence of large on-site correlation and exchange energies, the t_{2g} and e_g designations may not be very useful since combinations of these orbitals form each multiplet.

It is useful to try to forge a connection between phenomenological ground-state labels like $t_{2g}(\downarrow)$ and final-state multiplets. In the case of $t_{2g}(\downarrow)$ there is an obvious connection. When the $t_{2g}(\downarrow)$ electron is photoemitted from the left panel in Fig. 1, the final state is the high spin d^5 configuration and this is simply the ${}^6A_{1g}$ multiplet as shown in Fig. 3. In the same way, the $e_g(\uparrow)$ ground state maps into the ${}^4A_{1g}$, the ${}^4T_{2g}$, and the ${}^4T_{1g}$ final-state multiplets. These are the three lowest energy multiplets after the ${}^6A_{1g}$ ground state. Finally, the higher energy ${}^4T_{1g}$ and ${}^4T_{2g}$ multiplets are associated with emission from the $t_{2g}(\uparrow)$ state. In this way, we see that the left panel in Fig. 1 apparently can maintain some validity in interpreting the photoemission spectra.

B. Limitations of the localized model

The above description does not argue against the local model, but it does suggest redefinition of terminology. However, we distinguish five pieces of evidence that indicate the limitations of the ionic model.

(a) The finite Néel temperatures for $FePS_3$ and other MPX_3 compounds implies that intersite exchange interactions are small but not negligible. It is not clear whether the magnetic interactions are direct or indirect (i.e., superexchange). However, they imply significant hybridization of some sort.

(b) The calculated valence of $FePS_3$,[21] which matches the experimentally observed magnetic structure,[14] is $Fe^{0.95+}P^{1.47+}S_1^{0.70-}(S_2^{0.86-})_2$ (S_1 ion has no spin polarization, while S_2 does). The calculated self-consistent Mulliken's charges thus deviate substantially from the ionic model $M_2^{2+}(P_2S_6)^{4-}$.

(c) The Racah B and C parameters are smaller than for other more ionic iron compounds. The degree of covalency between Fe $3d$ and ligand p orbitals cannot be precisely determined. However, a larger degree of covalency in $FePS_3$ compared to iron compounds having more electronegative ligands would imply that the mean radial displacement of the Fe $3d$ electrons and thus the overall ionic size would increase. This will naturally decrease the Racah B and C parameters, which are governed by interelectron repulsion. In other words, a decrease in B and C is explicitly connected to delocalization of the $3d$ orbitals.

(d) The Fano asymmetry parameters vary systematically through the $3d$ manifold. This can be described in terms of hybridization of the multiplets with anion $3p$ orbitals and thus in terms of $3d$ delocalization.

(e) Significant dispersion is observed in the lowest of the Fe $3d$ features, A_3. This can only result through hybridization with neighboring ligands, or possibly with neighboring iron atoms. The overall bandwidth of roughly 1 eV is comparable to the multiplet splittings, which in turn are related to the phenomenological on-site correlation energy U.

Unlike the first three arguments, which do not inherently distinguish the localization of one $3d$ level from another and thus relate to "central-field covalency," the differential interaction implied by the last two is of relevance to "symmetry-restricted covalency." This was the primary conclusion of the extended Hückel calculations, i.e., that the interaction between the e_g orbitals and the sulfur ligands was large, while the t_{2g} orbitals remained nonbonding.[18,19] The different overlap between the t_{2g} and e_g orbitals with ligands will cause differential d-electron delocalization effects and hence possibly different effective Racah parameters for the different symmetry $3d$ orbitals.[41] These two covalency mechanisms are summarized to the nephelauxetic effect[48] which increases as $(1-\beta)$ increases in Table I. There is a close parallel between the nephelauxetic effect and Pauling's electronegativities. As the electronegativity of O, Cl, and S atoms decrease in sequence, the nephelauxetic effect increases.

C. Models for the electronic structure of $FePS_3$

We are left with a fairly complicated situation in which all interactions—the on-site correlation energy, the crystal-field interaction, multiplet splittings, and the bandwidth—are of comparable magnitude. More precisely, the interplay between these depends sensitively upon the $3d$-derived feature being considered. It is probably a good approximation to consider A_1 to be the $t_{2g}(\downarrow)$ level or ${}^6A_{1g}$ multiplet, perhaps split by the trigonal distortion. This assignment is valid since the band exhibits a bandwidth that is small compared to multiplet and crystal-field splittings. For this reason, the local model will adequately represent this feature. Given that A_3 is the most dispersive feature, it is natural, based upon symmetry-restricted covalency, to associate it with a hybrid band formed between the $e_g(\uparrow)$ and S $3p$ orbitals. This assignment is more problematic since the observed bandwidth for A_3 is comparable to the multiplet splittings and thus an assignment in terms of a particular local orbital is dubious. All multiplets contain some e_g character, and the concept of symmetry-restricted covalency may not be useful in this circumstance. By default, A_2 is assigned to the $t_{2g}(\uparrow)$ band and is apparently fairly localized, as expected based upon symmetry and as evidenced by its on dispersive nature. This model thus inverts the ordering of the $t_{2g}(\uparrow)$ and $e_g(\uparrow)$ orbitals in the left panel of Fig. 1. The fit in Fig. 3, coupled to the correlation between these orbitals and their final-state

multiplets discussed in Sec. IV A implies that this assignment is not valid.

These complications suggest consideration of different models for the electronic structure of $FePS_3$. It is useful to consider a purely energetic mechanism to explain the different degrees of localization in the 3*d* manifold. The electronic structure of $FePS_3$ can be considered to combine a strongly bonded P, S 3*p* manifold having a gap ~ 3 eV in magnitude with quasilocalized Fe 3*d* levels in and near the gap. The degree of localization of a particular multiplet will depend on its position in the gap: those far from the band edges (e.g., A_1) will be highly localized, while those close to the band edges or even outside the gap (e.g., A_3) will interact more strongly. This makes sense from a molecular orbital point of view because levels that are widely separated in energy generally mix less strongly than those that are nearly degenerate. This argument correctly predicts the qualitative observation that A_3 shows significant dispersion while A_1 and A_2 do not.

The above comments provide insight into the best way to think qualitatively about the electronic structure of these interesting, quasi-2D materials. They also indicate possible directions for future attempts to model their electronic structures. For example, in future calculations it would make sense to construct a basis set for the 3*d* levels starting from atomic multiplets, the splitting of which is governed by Racah parameters. The primary difficulty in such an approach is that the importance of the correlation interactions should be measured against solid-state hybridization effects, which apparently are very different for the different multiplets.

ACKNOWLEDGMENTS

This work was carried out in part at the NSLS at Brookhaven National Laboratory which is supported by the U.S. Department of Energy, Division of Materials Science and Division of Chemical Sciences. Financial support from the U.S. DOE under Grant No. DE-FG06-86ER45275. Won-Kook Choi was supported by Rotary International. We are deeply indebted to David Cleary of Washington State University for supplying the $FePS_3$ sample.

*Corresponding author. FAX: 503-346-3422. Phone: 503-346-4742 (office). Electronic address: kevan@oregon.uoregon.edu

[1]H. Ehrenreich and D. Turnbull, *Solid State Physics* (Academic, Boston, 1989).
[2]P. Fulde, *Electron Correlations in Molecules and Solids* (Springer, Berlin, 1991).
[3]W. Klingen, R. Ott, and H. Hahn, Z. Anorg. Allg. Chem. **396**, 271 (1973).
[4]W. Klingen, G. Eulenberger, and H. Hahn, Z. Anorg. Allg. Chem. **401**, 97 (1973).
[5]R. H. Friend and A. D. Yoffe, Adv. Phys. **36**, 1 (1987).
[6]F. S. Khumalo and H. P. Hughes, Phys. Rev. B **2**, 5375 (1981).
[7]M. Piacentini, F. S. Khumalo, G. Leveque, C. G. Olson, and D. W. Lynch, Chem. Phys. **72**, 61 (1982).
[8]M. Piacentini, F. S. Khumalo, C. G. Olson, J. W. Anderegg, and D. W. Lynch, Chem. Phys. **65**, 289 (1982).
[9]V. Grasso, S. Santangelo, and M. Piacentini, Solid State Ionics **20**, 9 (1986).
[10]N. Nagasudaram and A. H. Francis, J. Phys. Chem. Solids **50**, 163 (1989).
[11]G. Le Flem, R. Brec, G. Ouvrard, A. Louisy, and P. Segransan, J. Chem. Phys. Solids **43**, 455 (1982).
[12]M. Piacentini *et al.*, Solid State Commun. **51**, 467 (1984).
[13]V. Grasso, S. Santangelo, and M. Piacentini, Solid State Commun. **60**, 381 (1986).
[14]R. Brec, in *Intercalation in Layered Materials*, edited by M. S. Dresselhaus (Plenum, New York, 1986).
[15]K. Kurosawa, S. Saito, and Y. Yamaguchi, J. Phys. Soc. Jpn. **53**, 3919 (1983).
[16]M. Bernasconi *et al.*, Phys. Rev. B **38**, 12 089 (1988).
[17]E. Puppin, M. Scagliotta, and C. Chemilli, Solid State Commun. **78**, 905 (1991).
[18]M.-H. Whangbo, R. Brec, G. Ouvrard, and J. Rouxel, Inorg. Chem. **24**, 2459 (1985).
[19]H. Mercier, Y. Mathey, and E. Canadell, Inorg. Chem. **26**, 963 (1987).
[20]N. Kurita and K. Nakao, J. Phys. Soc. Jpn. **58**, 232 (1989).
[21]N. Kurita and K. Nakao, J. Phys. Soc. Jpn. **58**, 610 (1989).
[22]A. Aruchermy, H. Berger, and F. Levy, J. Solid State Chem. **72**, 316 (1988).
[23]V. Grasso, F. Neri, S. Pantanè, L. Silipigni, and M. Piacentini, Phys. Rev. B **42**, 1990 (1990).
[24]M. Piacentini *et al.*, Nuovo Cimento, Ser. ID **4**, 444 (1984).
[25]Y. Tanabe and S. Sugano, J. Phys. Soc. Jpn. **9**, 753 (1954).
[26]R. Nitsche and P. Wild, Mater. Res. Bull. **5**, 419 (1970).
[27]S. D. Kevan, Rev. Sci. Instrum. **54**, 1441 (1983).
[28]P. Thiry *et al.*, Nucl. Instrum. Methods **222**, 85 (1984).
[29]D. E. Eastman and J. L. Freeouf, Phys. Rev. Lett. **34**, 395 (1975).
[30]T. Ishii *et al.*, Phys. Rev. B **12**, 4320 (1975).
[31]J. J. Yeh and I. Lindau, Atomic Nucl. Data Tables **32**, 1 (1985).
[32]M. K. Kelley, R. R. Daniels, G. Margaritondo, and F. Lévy, Solid State Commun. **50**, 233 (1984).
[33]R. Rosencwaig, G. K. Wertheim, and H. J. Guggenheim, Phys. Rev. Lett. **27**, 479 (27).
[34]K. S. Kim, Chem. Phys. Lett. **26**, 234 (1974).
[35]K. S. Kim, J. Electron. Spectrosc. Relat. Phenom. **3**, 217 (1974).
[36]L. Orgel, *An Introduction to Transition Metal Chemistry* (Wiley, New York, 1966).
[37]P. S. Bagus, J. L. Freeouf, and D. E. Eastman, Phys. Rev. B **15**, 3661 (1977).
[38]S. Sugano, Y. Tanabe, and H. Kamimura, *Multiplets of Transition Metal Ions in Crystals* (Academic, New York, 1970).
[39]S. Koido and M. H. L. Pryce, Philos. Mag. **3**, 607 (1958).
[40]S. Alvarado, M. Erbudak, and P. Munz, Phys. Rev. B **14**, 2740 (1976).
[41]A. B. P. Lever, *Inorganic Electronic Spectroscopy* (Elsevier, New York, 1968).
[42]L. C. Davis and L. A. Feldkamp, Phys. Rev. B **23**, 6329

(1981).
[43]R. E. Deitz, Y. Yafet, G. P. Williams, G. P. Lapeyre, and J. Anderson, Phys. Rev. B **24**, 6820 (1981).
[44]S.-J. Oh, J. W. Allen, I. Lindau, and J. C. Mikkelsen, Phys. Rev. B **25**, 4845 (1982).
[45]S. Shin *et al.*, J. Phys. Soc. Jpn. **51**, 906 (1982).
[46]A. Kakizaki *et al.*, Phys. Rev. B **28**, 1026 (1983).
[47]B. D. Bartolo, D. Pacheco, and V. Goldberg, *Spectroscopy of the Excited State* (Plenum, New York, 1976).
[48]M. Gerloch and R. C. Slade, *Ligand Field Parameters* (Cambridge University Press, London, 1973).
[49]P. S. Bagus, C. R. Brundle, T. J. Chaung, and K. Wandelt, Phys. Rev. Lett. **39**, 1229 (1977).